Chapter III

Structure, Photocatalytic Degradation and Biocompatibility Studies of TiO_2 Nanoparticles and TiO_2-Cement Composite

3.1 Introduction

In this chapter the structural, microstructural, photocatalytic properties and biocompatibility of TiO_2 nanoparticles synthesized through sol-gel technique are discussed. Section 3.2 describes the structural and microstructural properties of TiO_2 nanoparticles calcined at 500 ºC. Photocatalytic properties of TiO_2 nanoparticles discussed in Section 3.3. Section 3.4 describes the biocompatibility of TiO_2. In addition to structural, photocatalytic and biocompatibility studies of TiO_2 nanoparticles, the photocatalytic properties of TiO_2 with cement are discussed in Section 3.5. Section 3.6 summarizes the experimental findings.

3.2 Structure and Microstructure of TiO_2 Nanoparticles

Structure and microstructure of TiO_2 nanoparticles are examined through XRD, Raman, SEM and TEM measurements. Figure 3.1 (a) depicts the X-ray powder diffraction pattern of the synthesised TiO_2 sample calcined at 500 ºC. Each peak is well resolved and the XRD pattern is in excellent agreement with JCPDS PDF#894921 corresponding to the anatase phase of TiO_2. No peak corresponding to rutile or brookite phase is observed. Average crystallite size of TiO_2 is calculated using Scherrer's equation for (101) peak which is found to be 33±0.003 nm. Raman spectroscopy is used to study surface features of the synthesized sample and result is shown in Figure 3.1 (b). Five Raman active modes are

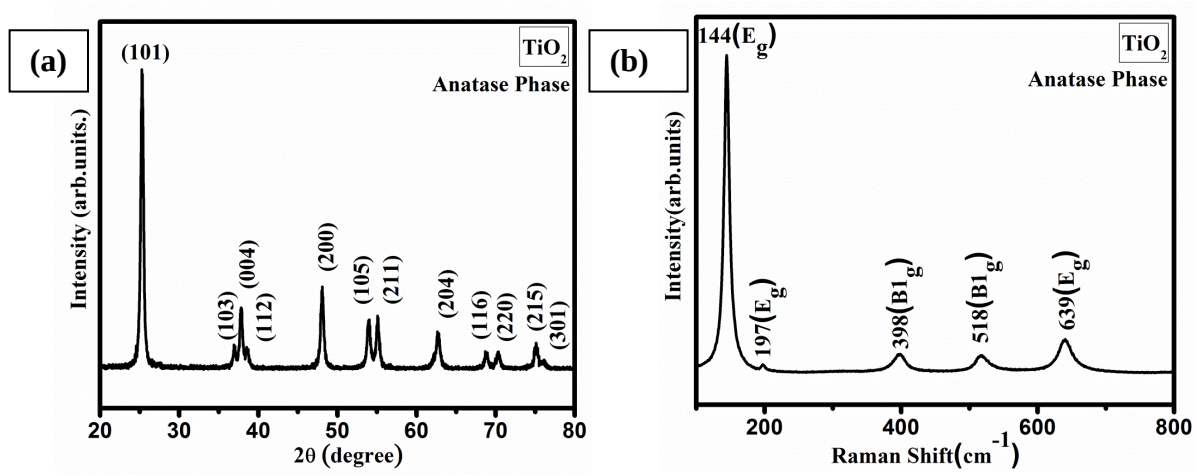

Figure 3.1 *(a) XRD pattern of TiO_2 synthesised by sol-gel route post calcined at 500 ºC, (b) Raman spectrum of TiO_2.*

observed. The observed bands are 144(E_g), 197(E_g), 398($B1_g$), 518($B1_g$), 642(E_g) which are match well with the anatase phase of TiO_2 [Hu et al. (2003)b and Bharati et al. (2017)]. Figure3.2 (a) and 3.3 (a) depict the scanning electron and transmission electron micrographs of synthesised anatase TiO_2 nanoparticles. Figure 3.2 (b) and 3.3 (b) show the particle size distribution histogram after calculating the size using Image J software. Further, histograms are fitted with Lorentzian function. From histograms, while majority of the particles are found to be in the range of 95 to 115 nm obtained from SEM, distribution of particles obtained from TEM, indicate the majority of particles in range of 45 to 65 nm. Both results are found to be higher than the crystallite size calculated from XRD line width. Combining the results obtained from SEM, TEM and crystallite size, we confirm that the TiO_2 nanoparticles are agglomerated and polycrystalline in nature. From HRTEM, we observe the lattice fringe spacing of 0.35 nm which corresponds to (101) plane of anatase phase of TiO_2 nanoparticles (Figure 3.3 (c)). Selected area electron diffraction pattern shown in Figure

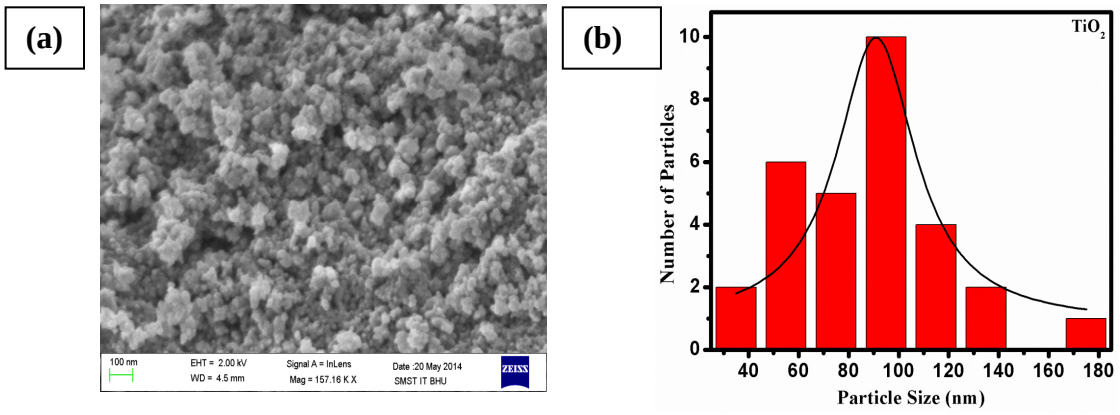

Figure 3.2 *(a) Field emission scanning electron micrograph of synthesised TiO_2 sample calcined at 500 ºC, (b) The corresponding particle size distribution histogram.*

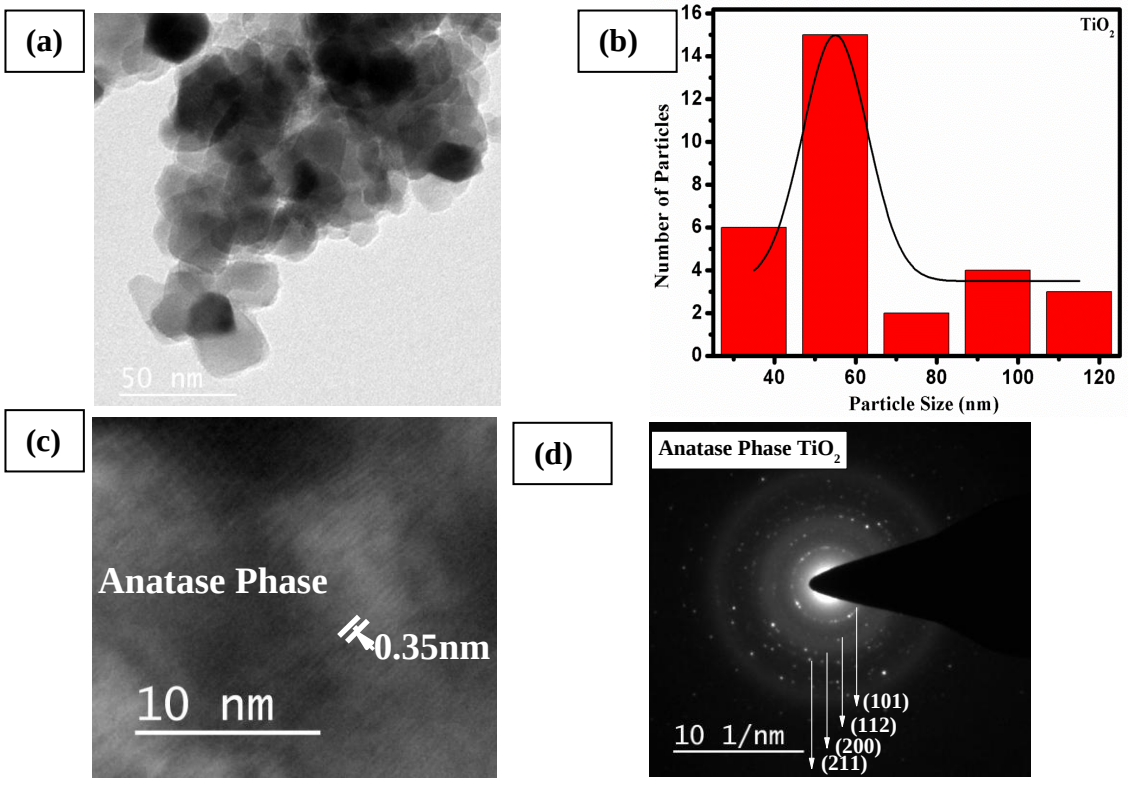

Figure 3.3 *(a) TEM image of synthesised TiO_2 sample calcined at 500 ºC, (b) the corresponding particle size distribution histogram, (c) shows the HRTEM image (d) shows the typical SAED pattern of the sample.*

3.3(d) further indicates the diffraction rings corresponding to (101), (112), (200), (211) of anatase phase. The result of HRTEM analysis is consistent with that of the XRD results.

3.3 Photocatalytic Property of TiO_2 Nanoparticles

Figure 3.4 (a) depicts room temperature optical absorbance spectrum of synthesised TiO_2 nanoparticles. The absorption spectrum is broad and exhibits strong absorption at around 400 nm. The broad absorption peak could be due to broad particle size distribution. Since anatase TiO_2 is an indirect band gap semiconductor, a plot of $(\alpha h\nu)^{1/2}$ as a function of photon energy (E), yields a linear dependence assuming parabolic band dispersion. This is a good approximation to determine band gap, E_g. The band gap calculated by extrapolating the linear portion of the curve as shown in Figure 3.4 (b) which is found around ~3.15 eV. The band gap of anatase TiO_2 is less than that of bulk TiO_2 (3.2 eV). In contrast to reported literatures where band gap increases with decrease in size, the decrease in E_g in present case is due to agglomeration of nanoparticles. Moreover, decrease in band gap shifts the band edge towards the visible range which is important from absorption point of view.

It is known that one of the most popular photocatalyst, TiO_2 have long been investigated in environmental purification and decomposition of dyes in waste water [Fujishima et al. (1972), Arbuj et al. (2010), Jiao et al. (2013) and Trabelsi et al. (2012)]. Among rutile, brookite and anatase phase of TiO_2, anatase TiO_2 has attracted more attention for its use as photocatalyst in response to its application in environmental related problems [Asilturk et al. (2006)]. Zhang et al. (2011) show the degradation of acid red G (ARG) and 4-nitrophenol under UV light using composites of TiO_2 and clay. Efficient photocatalytic activity attributed to the synergetic effect of large surface area [Zhang et al. (2011)a, Zhang

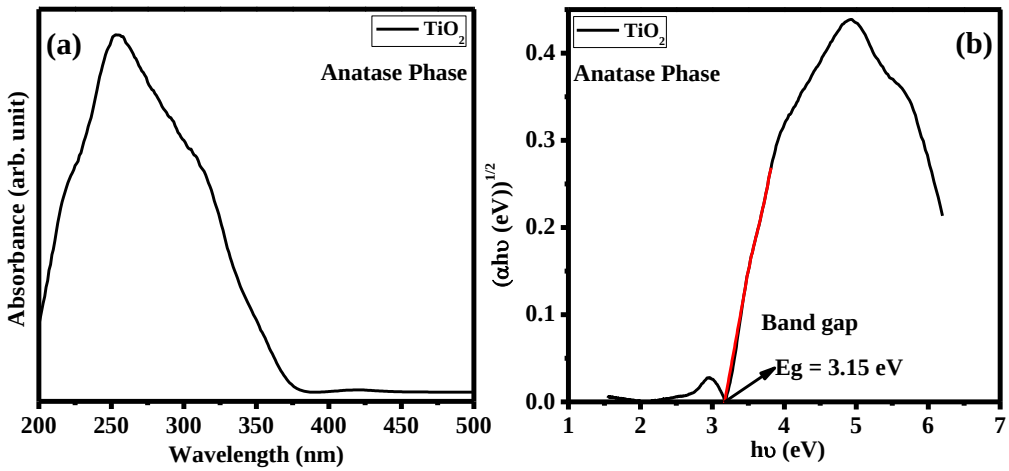

Figure 3.4 *(a) Absorbance spectrum of TiO_2 nanoparticles calcined at 500 ºC, with broad absorbance (b) The dependence of $(\alpha h\nu)^{1/2}$ on the incident photon energy ($h\nu$) for TiO_2.*

et al. (2011)b and Zhang et al (2011)c]. Yu et al. (2016) synthesized CTAB@BiOCl and used for eliminating dye contamination by degrading Reactive Red 3 and Congo Red. Photocatalytic activity enhanced due to increasing absorptivity of the composite material. Guo et al. (2012) observed that organic contaminant, Rhodamine B has been degrade 4.5 times faster by using composite of $CaWO_4/Bi_2WO_6$ than that of pure Bi_2WO_6 . Being TiO_2 nanoparticles synthesised by sol-gel route show anatase phase in the present case, therefore, we proceed to study the photocatalytic activity under UV (254 nm) and renewable source of light i.e sunlight. It is important to examine the degradation of residual dyestuff that mainly comes from textile and photographic industry which is one of the major sources of environmental contamination [Zhang et al. (2011)a,b,c, Guo et al. (2012) and Yu et al. (2016)]. Within overall category of dye stuffs, Rhodamine B (RhB), one of the xanthene dye, Congo Red, a well known azo dye and Methylene Blue, a well know thiazine dye are

of common organic pollutants. In this chapter, we study the purification of dye effluent using TiO_2 nanoparticles.

Absorbance is measured by irradiating the mixture of TiO_2 and different dye solutions such as MB, CR and RhB with UV and sunlight for different time periods. We measure absorbance of MB, CR and RhB before and after irradiating with UV light shown in Figure 3.5 (a), (b) and (c). The absorbance maxima are generally observed at 664 nm, 502 nm and 548 nm for MB, CR and RhB, respectively [Arbuj et al (2010), Edemoglu et al. (2008), Asilturk et al. (2006)]. The absorbance maxima (λ_{max}) observed at 663 nm, 499 nm and 554 nm for MB, CR and RhB, respectively after UV-irradiation, corroborated with the above reported literatures. Intensity of the absorbance maxima decreases with increasing time of irradiation indicating the decrease in concentration of dye solutions, shown as insets of Figure 3.5 (a), (b) and (c). While in case of MB and RhB, intensity of absorbance maxima is completely disappeared after 180 min of irradiation, in CR, the absorbance maxima is disappeared after 120 min. Figure 3.5 (d), (e) and (f) show the pictorial representation of degraded dyes, MB, CR and RhB solutions respectively with increasing irradiation time under UV light (from left to right). One may notice the change in color of dyes to colorless with respect to time of irradiation. The absorbance spectra of MB, CR and RhB, before and after irradiating with sunlight are shown in Figure 3.6 (a), (b) and (c), respectively. We have observed absorbance maxima (λ_{max}) at 658 nm, 499 nm and 553 nm for MB, CR and RhB**,** respectively, match with the absorbance maxima measured under UV-irradiation. The intensity of absorbance maxima almost disappear after 90 min, 45 min and 180 min of irradiation in MB, CR and RhB respectively. Figure 3.6 (d), (e) and (f) show the pictorial representation of degraded dyes, such as, MB, CR and RhB solutions, respectively with

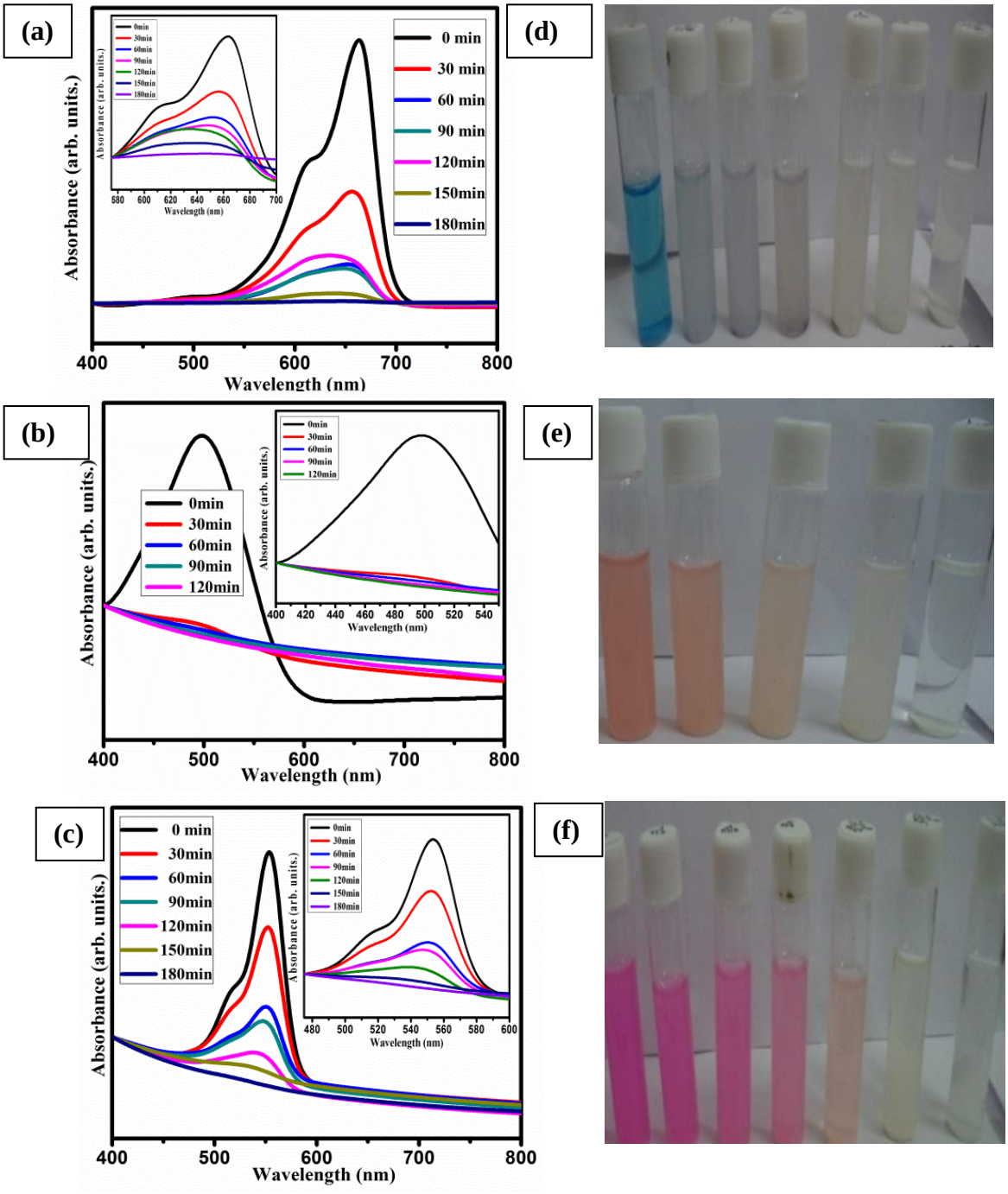

Figure 3.5 *Time dependant degradation of MB, CR and RhB solution with photocatalyst TiO_2, before and after UV-irradiation; UV-Visible absorption spectra of dye solutions (a) MB, (b) CR, (c) RhB and Pictorial representation of degrade dye solution with increasing irradiation time (from left to right) (d) MB, (e) CR, (f) RhB.*

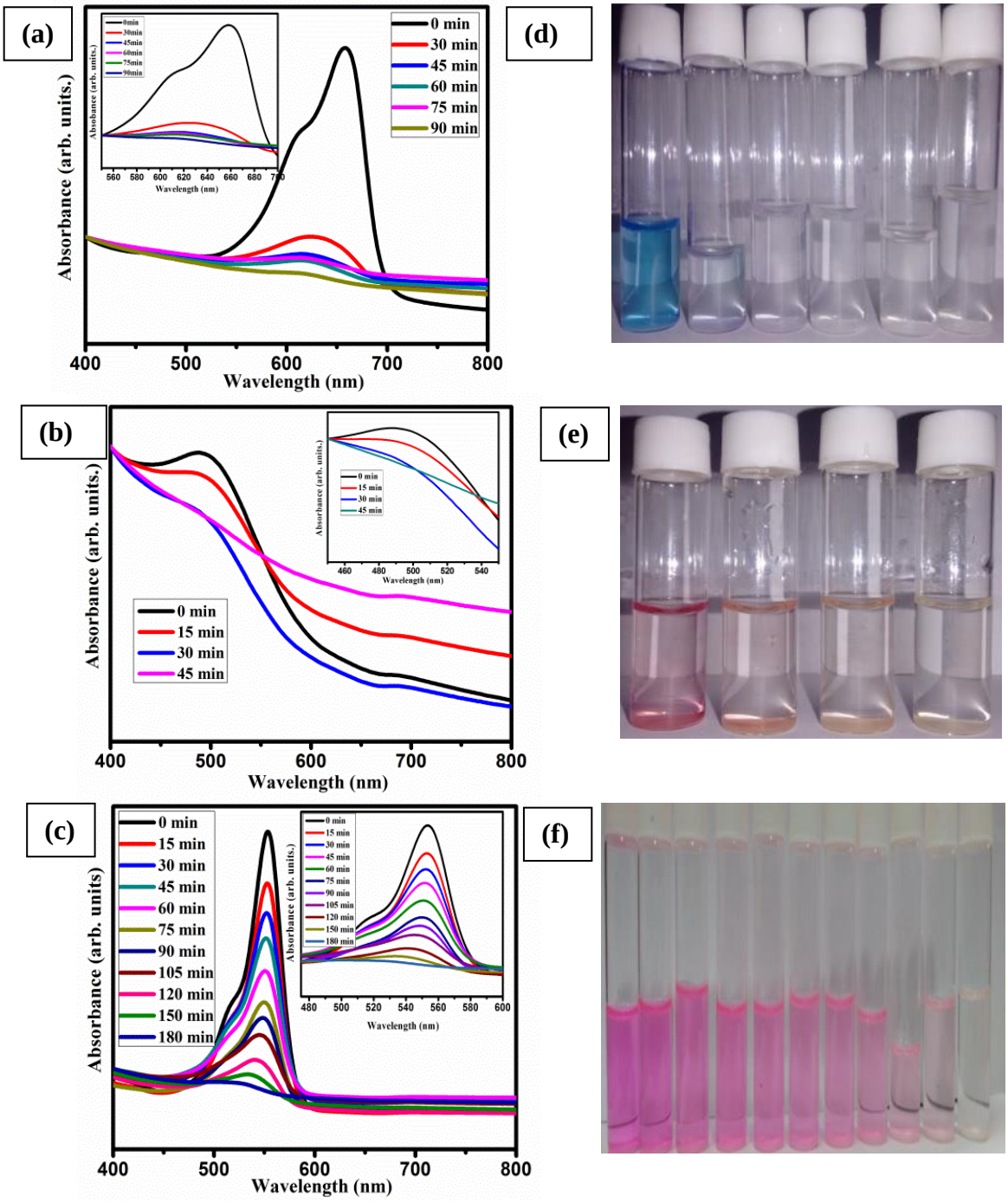

Figure 3.6 *Time dependant degradation of MB, CR and RhB solution with photocatalyst TiO_2, before and after sunlight irradiation; UV-Visible absorption spectra of dye solutions (a) MB, (b) CR, (c) RhB and Pictorial representation of degrade dye solution with increasing irradiation time (from left to right) (d) MB, (e) CR, (f) RhB.*

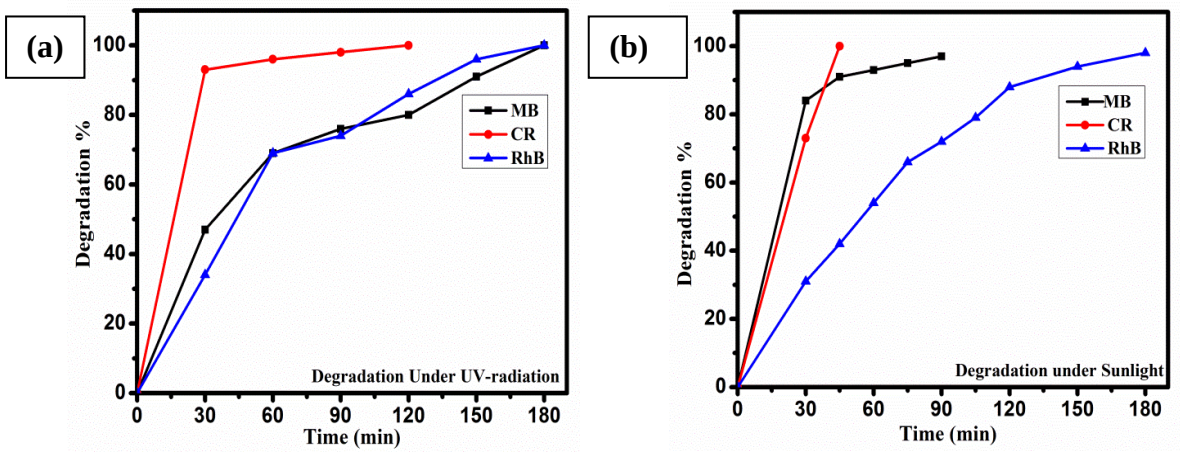

Figure 3.7 *Degradation percentage; (a) under UV (b) under sunlight.*

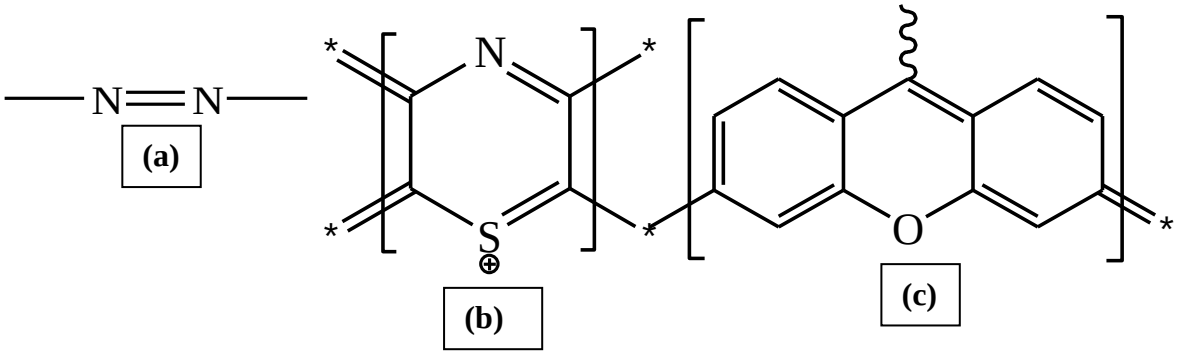

Figure 3.8 *The chromophores in CR, MB and RhB are (a) Azo gr**o**up, (b) Thiazine group and (c) Xanthene group respectively.*

increasing irradiation time under sunlight. The colorful solutions become colorless due to the cleavage of C-C, C-N, C-S and -N=N- bonds. Further, we have calculated the percentage of degradation of the dyes. The degradation percentage of the dyes with irradiation time under UV-light is shown in Figure 3.7 (a). While 100% degradation of MB and RhB are obtained after 180 min of irradiation, 100% degradation of CR is observed after 120 min. Figure 3.7 (b) depicts the degradation percentage with irradiation time under sunlight. We

have observed 97% degradation of MB after 90 min, 100% degradation of CR after 45 min and after 180 min**,** RhB degrades by 98%. In both the cases i.e under UV and sunlight we observe that CR degrades faster than MB and RhB. This could be due to the chromophore responsible for the color of the CR dye i.e smaller azo-group, whereas, in MB and RhB, chromophores are larger thiazine and xanthene groups. One may clearly see that while one needs the cleavage of -N=N- bond in CR, MB and RhB degradation needs to break more number of bonds like C-C, C-N, C-S and C-O with stable aromatic group for cleavage which is more time consuming as observed in the present case. The chromophores in CR, MB and RhB are Azo group, Thiazine group and Xanthene group, respectively which are depicted in Figure 3.8.

In literatures, although there are reports regarding degradation of above dyes using various forms of TiO_2 nanostructures, we have shown the degradation of above dyes of higher concentration within a time period which is less than the reported value under renewable source of light. In general, degradation depends upon various factors such as concentration of dye, concentration of catalyst, band gap energy and particle size of the catalyst. For example, dye concentration decides the screening of UV-light falling on the catalyst. Consequently, the generation of ˙OH radical at the surface of the catalyst is controlled. Higher the concentration of dye, lower is the generation of ˙OH radical on the surface of the catalyst, hence lower is the degradation rate [Asilturk et al. (2006) and Edemoglu et al. (2008)]. It has also been reported that in higher concentration of dye, the path length of photon generated by inducing UV light, may be reduced which contributes to degradation [Trabelsi et al. (2012)]. Some of the photons may be absorbed by the dye before reaching to the catalyst which can also reduce the efficiency of catalytic reaction [Dafare et

al. (2013) and Edemoglu et al. (2008)]. The concentration of catalyst also plays an important role, such as for less concentration of catalyst, it is insufficient for adsorption of dye on the surface of the catalyst. As a result, the rate of degradation decreases. If it is higher than the required concentration, the rate of degradation also decreases due to (i) sedimentation of the particles and (ii) deactivation of activated molecules [Asilturk et al. (2006)]. In addition to the above factors, band gap of the catalyst decides the generation of electron-hole pairs and their recombination. If the energy of irradiation is higher than the band gap energy, then it leads to recombination of electron and hole [Liu et al. (2009)]. As a consequence, it decreases the rate of degradation. If it is lower, excitation of electron from valence band to conduction band is hindered, results in decreasing hydroxyl radical. Reducing the size of the catalyst, the surface area increases which increases the adsorption area and hence the degradation of the dye. Shen et al. (2007) have shown that while N-doped TiO_2 thin films exposed with 405 nm semiconductor laser for 12 h shows 51% degradation of MB solution, using undoped TiO_2 thin films no degradation is achieved. Recently visible light driven photocatalytic degradation of less than 50% of RhB dye have been observed using Cr-doped $SrTiO_3/TiO_2$ hetero-structure nano-tube array after 4 h of irradiation with 300 W Xe lamp [Jiao et al. (2013)]. It has also found that TiO_2 nano-tube arrays coated with much thicker and densely packed Cr-doped $SrTiO_3$ nuclei could severely destroy the tubular structure and hinder the excellent electron transport ability of TiO_2 nano-tube array and results in decrease in photocatalytic ability. Arbuj et al. (2010) report that, 50 mg of mixed anatase and rutile phase TiO_2 nanoparticles used for degrading 100 ml of 10 ppm MB solution using mercury vapour lamp at about 30 min of irradiation. Fang et al. (2014) prepared Ti^{3+} self doped TiO_2 and used the sample for degradation of Rhodamine B under 500 W tungsten halogen lamp

and 300 W high pressure Hg lamp. The Ti^{3+} generation is responsible for enhanced visible light absorption and photocatalytic activity, which is beneficial to the production of ˙OH and other active groups. Shen et al. (2013) synthesised mixed anatase and brookite phase TiO_2 sample by hydrothermal method. Examined the degradation of Rhodamine B under 300 W high pressure Hg lamp. The mixed phase TiO_2 exhibits higher activity than the pure phase TiO_2. It have been reported by Zhang et al. (2003) and Dong et al. (2012), that the porous structure of catalyst responsible for increasing rate of photo reactivity as porosity increases the surface area. Li et al. (2016)b reported, presence of oxygen vacancy in catalyst facilitate the barrier less O-H bond breaking in proton removal reaction which leads photocatalytic degradation of organic contaminants. Li et al. (2014)b reported that photo reactivity is strongly depends on the magnitude of the internal electric field (IEF). More exposure could induce the generation of stronger IEF, consequently charge separation and transfer increases which enhance photoreactivity. However, our results show that only 20 mg of TiO_2 nanoparticles of anatase phase could degrade 5 ppm of MB and RhB solution at 90 min and 180 min, respectively under renewable source of light which is higher than the reported literatures reported so far. Therefore, among burgeoning literatures on photocatalytic studies using TiO_2 based materials, for first time we show higher degradation percentage of MB and CR under sunlight. However, in case of RhB, the degradation behavior under UV-light and sunlight is same. This indicates that TiO_2 nanoparticles in the present study degrade MB and CR more actively under sunlight than under UV-light. Because under UV light of 254 nm (4.8 eV) wavelength, although electrons easily excite from valence band to conduction band, the recombination of electron and hole reduces the degradation rate [Jiao et al (2013)].

In general, photocatalytic water oxidation is governed by proton removal reaction which involves both the O-H bond breaking and trapping of a photo generated hole (H_2O^* + $hole^+ \rightarrow$ ·OH* +·H) on the valence band. Diffusion of ·OH* species away from the surfaces allows generation of free ·OH radicals and H_2O_2 which are key component for removal of organic pollutant [Li et al. (2016)b]. Photocatalytic reaction entirely depends on the energy of light irradiated on the surface of material like TiO_2 in the present case. When the band gap matches with the wavelength of visible light, electrons are excited from valence band to the conduction band leaving holes on the valence band. Ultimately hole generated after irradiating with light significantly contributes to dissociate the H_2O to ·OH. Under sunlight due to broad particle size distribution as obtained from SEM and TEM analysis gives rise to wide absorption spectral range coincides with solar spectrum starting from 300 nm, higher than that of UV light (254 nm). It results into excitation of large number of electrons from valence band to conduction band and less recombination of electron and hole producing large number of hydroxyl radicals. Faster degradation could be due to more the hydroxyl radicals, produced in presence of TiO_2 having large surface to volume ratio.

The degradation profile follows apparent first-order kinetics which is strongly evident from the exponential decay curve as shown in Figure 3.9 (a) and (b) under UV and sunlight respectively. The process of degradation under sunlight using TiO_2 nanoparticles is cost effective and is less time consuming. Further, we have examined the biocompatibility of the synthesised TiO_2 and discussed in Section 3.4.

3.4 Biocompatibility of TiO_2

In order to use the water after photocatalytic degradation of dye effluents obtained from textile industries in agriculture and/or domestic sectors, it is important to know

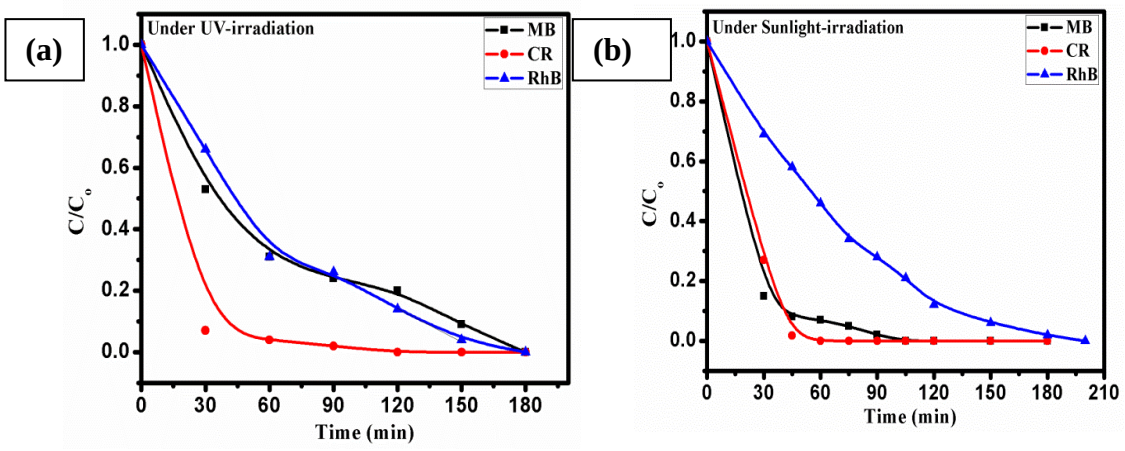

Figure 3.9 *First-order exponential decay curve of MB, CR and RhB, (a) under UV-irradiation, (b) under sunlight irradiation.*

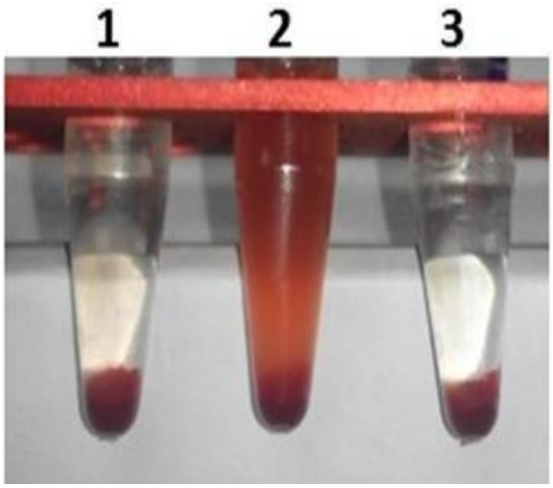

Figure 3.10 *Effect of TiO_2 on erythrocyte membrane integrity. RBC suspensions were exposed to TiO_2 for 3h followed by centrifugation. Red color indicates positive hemolysis. 1. Represents negative control, 2. Represents positive control, 3. Represents TiO_2 sample.*

the biocompatible nature of TiO_2 nanoparticles. Because since today, many reports suggest that nano TiO_2 could be absorbed through respiratory tract, digestive tract into the human body and distributed in such key organs [Wang et al. (2007) and Warheit (2007)]. TiO_2 can migrate along the body within blood before arriving at target organs, so the influence of nano TiO_2 on cells in blood should be paid more attention. Therefore, we study the interaction TiO_2 on blood platelets, its hemocompatibility and cytotoxicity through MTT assay to confirm the biocompatible nature of TiO_2.

3.4.1 Effect of TiO_2 on Erythrocyte Membrane Integrity

The most abundant cell population in blood is Red blood corpuscles (RBCs). As nanomaterials finding access into circulation would expose them to circulating platelets as well as RBCs, we have sought to determine the effect of TiO_2 on RBCs. Figure 3.10 depicts the results of hemolysis, where deionised water has been taken as negative control in vial-1, phosphate buffer saline (PBS) taken as positive control in vial-2 and the sample of TiO_2 taken in vial-3. Table 3.1 shows percentage of hemolysis results, calculated using the following equation:

$$\% \text{ Hemolysis} = \frac{\text{samples abs}_{540-655\text{nm}} - \text{negativecontrol abs}_{540\_655\text{nm}}}{\text{positivecontrol abs}_{540\_655\text{nm}} - \text{negativecontrol abs}_{540\_655\text{nm}}} \times 100 \quad \text{.....(3.1)}$$

Negative control, positive control and TiO_2 gives 0%, 100% and 0.002% hemolysis respectively. Both TiO_2 and negative control shows almost equivalent results. GO (Graphene oxide) has recently been reported to induce significant breakdown of the RBC

Table 3.1 *Percent hemolysis of RBCs incubated with TiO_2 is 0.002%, Positive control PBS is 100% and Negative control is 0%.*

Ratio	TiO_2	Positive Control	Negative Control
$1:10^7$ (Solution: PBS)	0.002	100	0

membrane leading to hemolysis [Singh et al. (2012)]. In contrast to GO, TiO_2 does not exhibit any hemolytic activity when one exposed to RBCs. We conclude that TiO_2 is a highly hemocompatible nanomaterial, which does not affect in circulation of blood cells rather maintains RBCs.

3.4.2 Effect of TiO_2 on Platelet Functions

Further we have studied the platelet interaction with TiO_2. Figure 3.11 shows platelet aggregation study of TiO_2 by taking thrombin as positive control. Addition of thrombin to the freshly isolated human platelets suspension trigger a strong wave of cell aggregation (amplitude 70±5%), however TiO_2 fails to induce any platelet aggregation (Figure 3.11), it has been reported that, while GO shows platelet aggregation, G-NH_2 (amine modified grapheme oxide) does not induce any platelet aggregation [Singh et al. (2011) and Singh et al. (2012)].

After studying hemolysis and platelet aggregation of TiO_2 nanoparticles, we proceed to examine the effect of TiO_2 on the level of intracellular ROS in human platelets. H_2O_2 is employed as positive control and N-acetylcysteine (NAC) taken as negative control. 2',7'-Dichloro dihydrofluorescein diacetate (H_2DCF-DA) loaded platelets are exposed to TiO_2,

negative control and positive control at 37 ºC for 10 min and change in fluorescence is recorded. Figure 3.12 (a) shows increase in cytosolic ROS when H_2O_2 is employed as

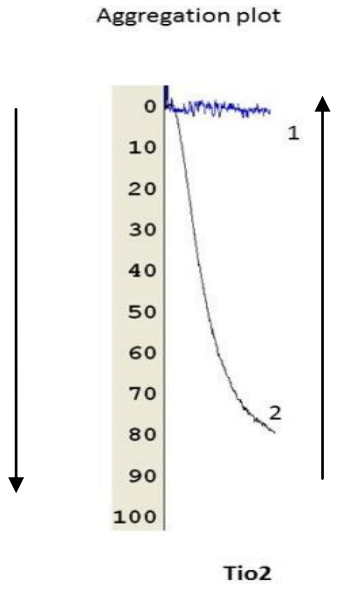

Figure 3.11 *Platelet aggregation induced by TiO_2. 1. Represents TiO_2 and 2. Represent thrombin.*

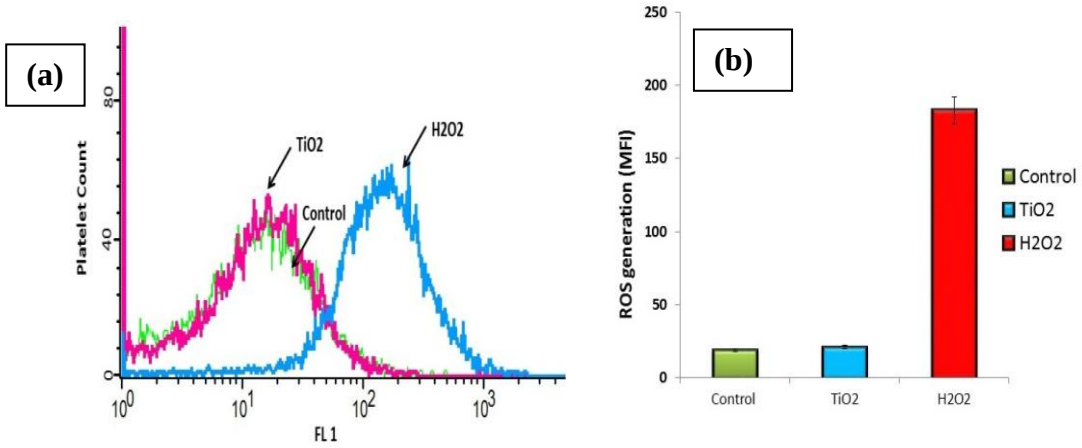

Figure 3.12 *(a) ROS generation in H_2DCF-DA loaded platelets treated TiO_2, H_2O_2 as positive control and NAC as negative control. Fluorescence was recorded at 530nm (excitation, 500nm). The results are representative of three independent experiments. (b) Histogram representation of ROS generation in, Control, TiO_2 and H_2O_2.*

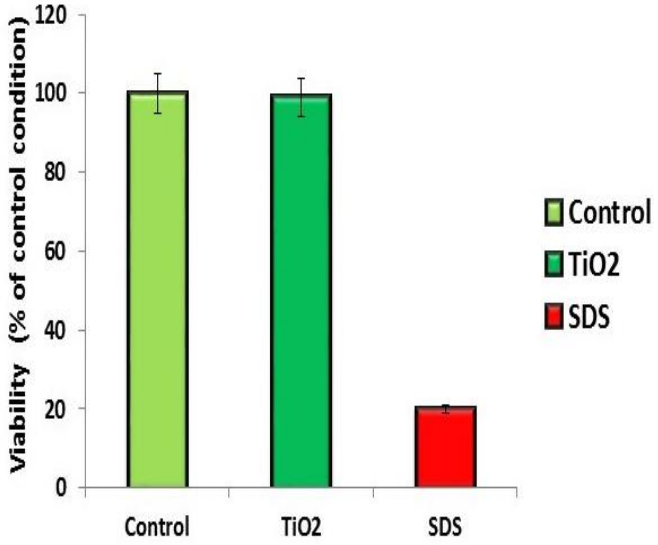

Figure 3.13 *MTT assay of TiO_2. SDS indicates the controlled experiment.*

positive control. The observed elevation in ROS is entirely scavenged by the reductant Nacetylcysteine (NAC). There is no significant change in ROS level in platelets exposed to TiO_2, which is almost equivalent to negative control. Figure 3.12 (b) shows histogram representation of ROS generation, when 2',7'- Dichlorodihydrofluorescein diacetate (H_2DCF-DA) loaded platelets are exposed to TiO_2, as well as negative control and positive control. The obtained results indicate that ROS generation by TiO_2 is equivalent to negative control. Contrasting this lower concentration of GO is sufficient to trigger enhancement in the level of cytosolic ROS [Singh et al. (2012)].

3.4.3 Cytotoxicity Assessment of TiO_2

In order to reaffirm the biocompatibility of TiO_2, we assess its cytotoxicity through MTT assay. MTT is known to be reduced to formazan in viable cells by mitochondrial

reductase, exhibiting a purple color. Formazan production was measured after 1 h exposure of platelets to TiO_2 against the control of untreated platelets. Figure 3.13 illustrates MTT assay of TiO_2. Sodium docyle sulphate (SDS) (1%)-treated platelets are used as positive control. TiO_2 does not exhibit cell death in MTT assay, as the results are almost equivalent to negative control. The results support the conclusion that TiO_2 does not exhibit any cellular toxicity, thus facilitates the use of TiO_2 nanoparticles as potential biomaterial. Hemolysis, ROS generation, platelet aggregation and cell viability studies confirm that TiO_2 nanomaterials are biocompatible material. Being nanoparticles of TiO_2 are good photocatalyst and good biocompatible material one may use it as agent for purifying the impure water. Further, we have fabricated TiO_2-cement composite pellets and studied the photocatalytic activity of the pellets under sunlight.

3.5 Photocatalytic Property of TiO_2-Cement Composite

Here we have fabricated the composite pellets with three different compositions, such as 50 mg TiO_2 and 20 mg cement is referred as TC1 whereas pellets with 50 mg cement with 20 and 10 mg TiO_2 as TC2 and TC3, respectively. Thereafter, we examined the photocatalytic activity of these pellets which is discussed below.

Before carry out photocatalytic analysis we have studied the morphology of the composite pellets. Figure 3.14 (a) shows the SEM image of cement comprised of layered structure with particle size of ~30 μm. However, TC1 shows lumps of agglomerated TiO_2 nanoparticles in between the cement particles which might be due to the excess amount of TiO_2 with lesser cement content shown in Figure 3.14 (b). On the other hand, TC2 contains uniformly distributed TiO_2 nanoparticles with the cement particles (Figure 3.14 (c)). Further,

the photocatalytic property of these TiO_2 and cement composites are studied in detail by degrading organic pollutants. TiO_2 is widely used for photocatalytic degradation of pollutants owing to excellent photocatalytic efficiency. Previously, we have examined the photocatalytic performance of anatase phase TiO_2 nanoparticles after degrading organic dyes like MB, RhB and CR under UV (254 nm) and sunlight [Bharati et al. (2017)]. It has been established that the higher degradation percentage is obtained under sunlight compared to UV providing an inexpensive process for cleaning of industrial waste water. To overcome the drawbacks of previous processes, the photocatalytic property of TiO_2 nanoparticles embedded in cement pellets has been investigated in detail. To assess the photocatalytic efficiency of composite pellets, 50 ml of dye solution is taken in a conical flask with composite pellets following irradiation with sunlight. Hereafter, aliquots of dye solution are collected in glass vials before and during irradiation of sunlight at every 30 min time interval. The absorbance spectra of collected samples reveal that the absorbance maxima (λ_{max}) for MB appear at ~665 nm which appear at wavelength range such as ~550 and ~500 nm for RhB and CR, respectively [Bharati et al. 2017]. With increasing irradiation time, the intensity of absorbance maxima decreases demonstrating reduction in the concentration of dye solution due to the presence of TiO_2 nanoparticles known to be photocatalytically active under sunlight. Figure 3.15 (a) depict the absorbance spectra of all three dye solutions, such as MB, RhB and CR before and after irradiating with sunlight using only one pellet of TC1 (50 mg TiO_2 and 20 mg Cement). The peak intensity of MB and CR almost disappears after 120 min of irradiation, whereas ~30 % of the peak intensity decreases in case of RhB. Figure 3.15 (b) show the pictorial representation of the degraded dye solutions with irradiation time

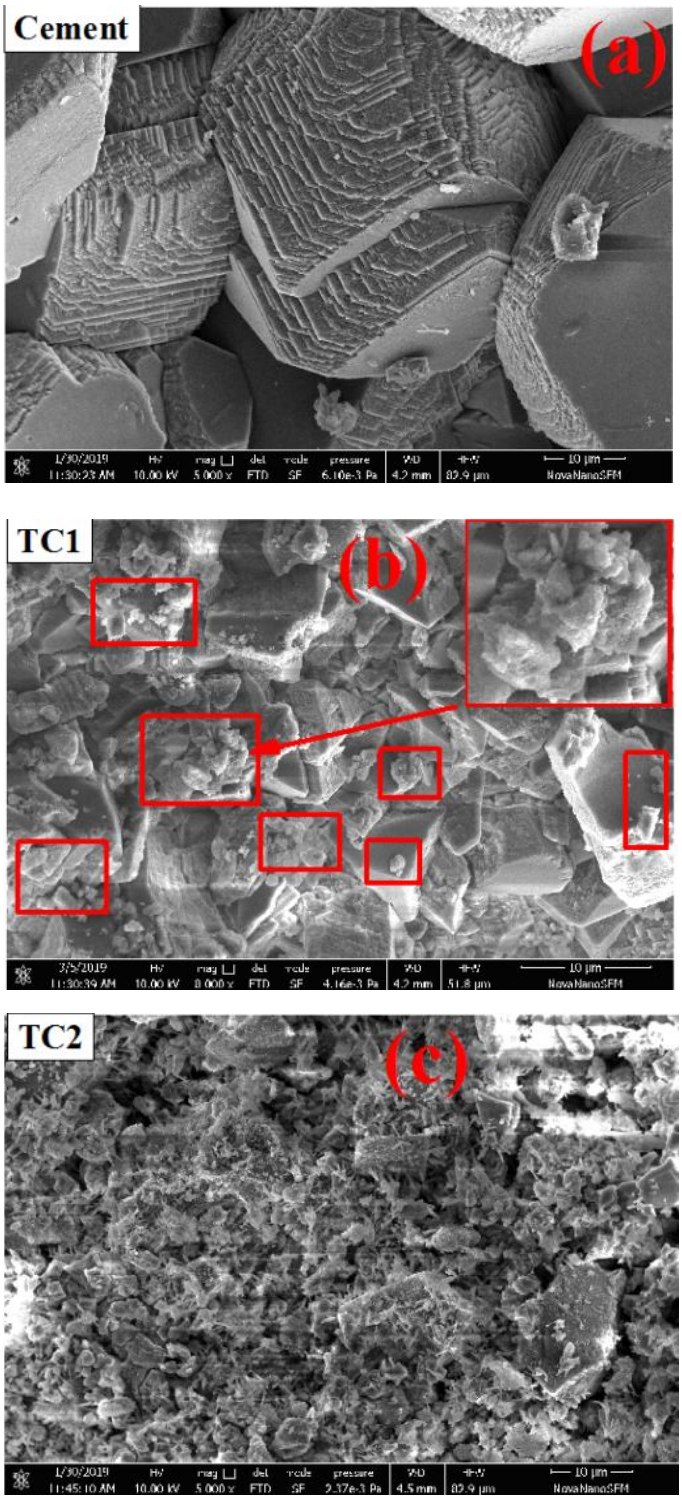

Figure 3.14 *HRSEM images of (a) cement, (b) and (c) cement and TiO_2 composites.*

(from left to right). It is easy to recognize the change in color from dark to bright for all three dyes with respect to irradiation time. Figure 3.15 (c) represents the estimated degradation percentage of dye solutions after 120 min of irradiation indicating ~100, ~95 and ~35% degradation of CR, MB and RhB, respectively. Despite the fact that the results are promising, the pellets are not strong enough in terms of strength and rigidity since the pellets dissociate partially after 120 min of irradiation. Such dissociation of the pellets could be due to the composition ratio containing higher amount of TiO_2 i.e. 50 mg. The observed lumps of TiO_2 can create some adhesive forces due the Van der Waals interactions between TiO_2 particles and cement as well as TiO_2 particles itself. Therefore, we focus over fabricating pellets with improved strength by increasing amount of cement i.e. 50 mg with reduced amount of TiO_2 such as 10 and 20 mg. Thereafter, the photocatalytic property of modified composition pellets are examined by degrading same dyes as above. Figure 3.16 and 3.17 compare the absorbance spectra of all three non irradiated and irradiated dyes using catalyst TC2 and TC3 with four pellets each. The degradation rate becomes almost half of earlier reaction as this composition require double time (4 h) to degrade ~100, ~30 and 90% of MB, RhB and CR, respectively shown in Figure 3.16 (c) and 3.17 (c). When sunlight is incident on the TiO_2 nanoparticles embedded in cement pellets, the excitation of electrons takes place from valence band to conduction band. This excitation process generates certain electron and hole pairs. The excited electrons react with the oxygen producing superoxides, whereas the holes react with water resulting in formation of hydroxyl radicals. Because of the highly reactive nature of the radical species, they instantly react with the organic pollutants (dye effluents), harmful for environment. Finally, the degraded organic pollutants yield carbon

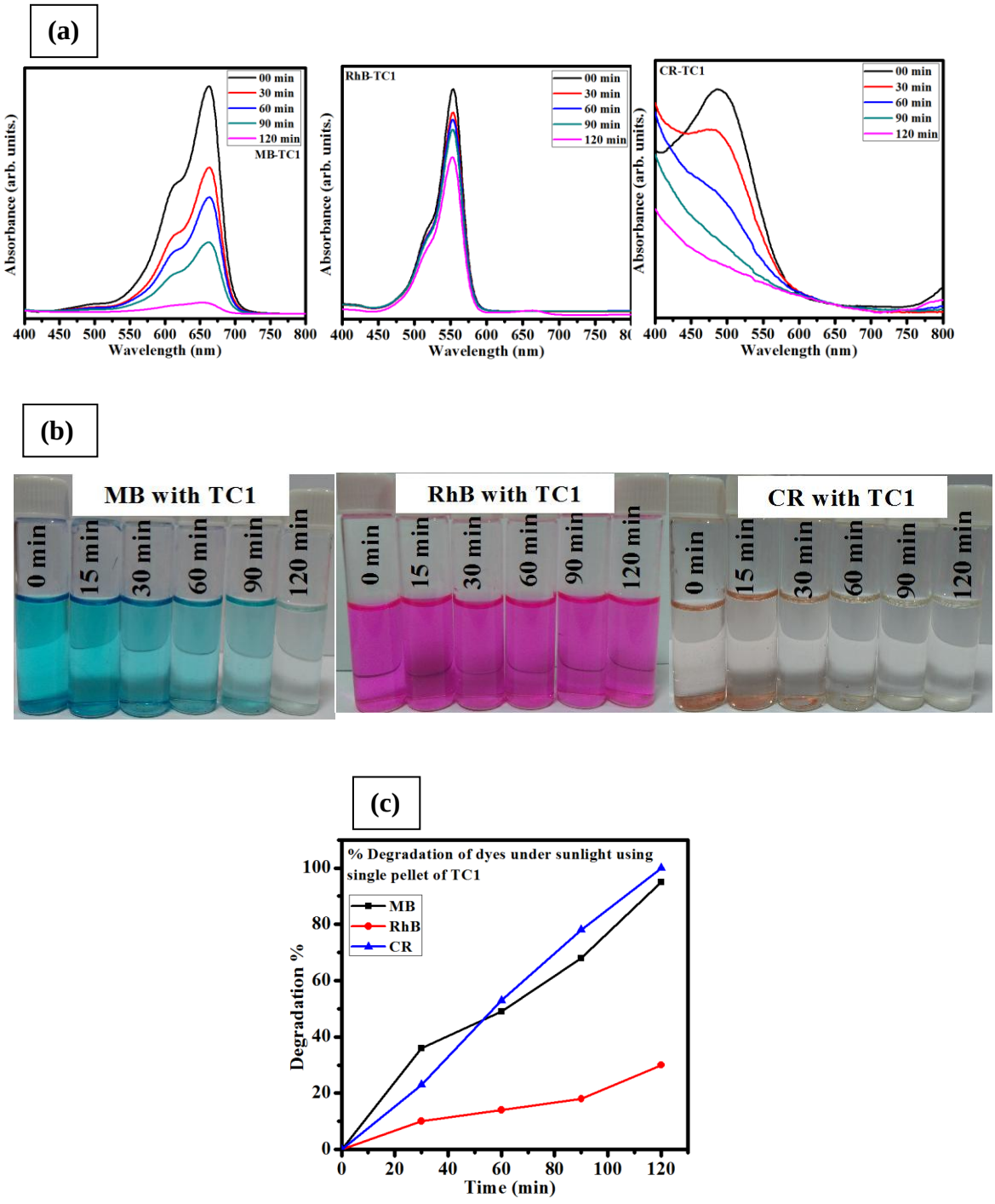

Figure 3.15 *(a) UV-visible absorption spectra of MB, RhB and CR, dye solutions with pellet TC1 before and after irradiating with sunlight, (b) show the pictorial representation of dye solutions from 0 min to 120 min (left to right) and (c) Degradation percentage of dyes.*

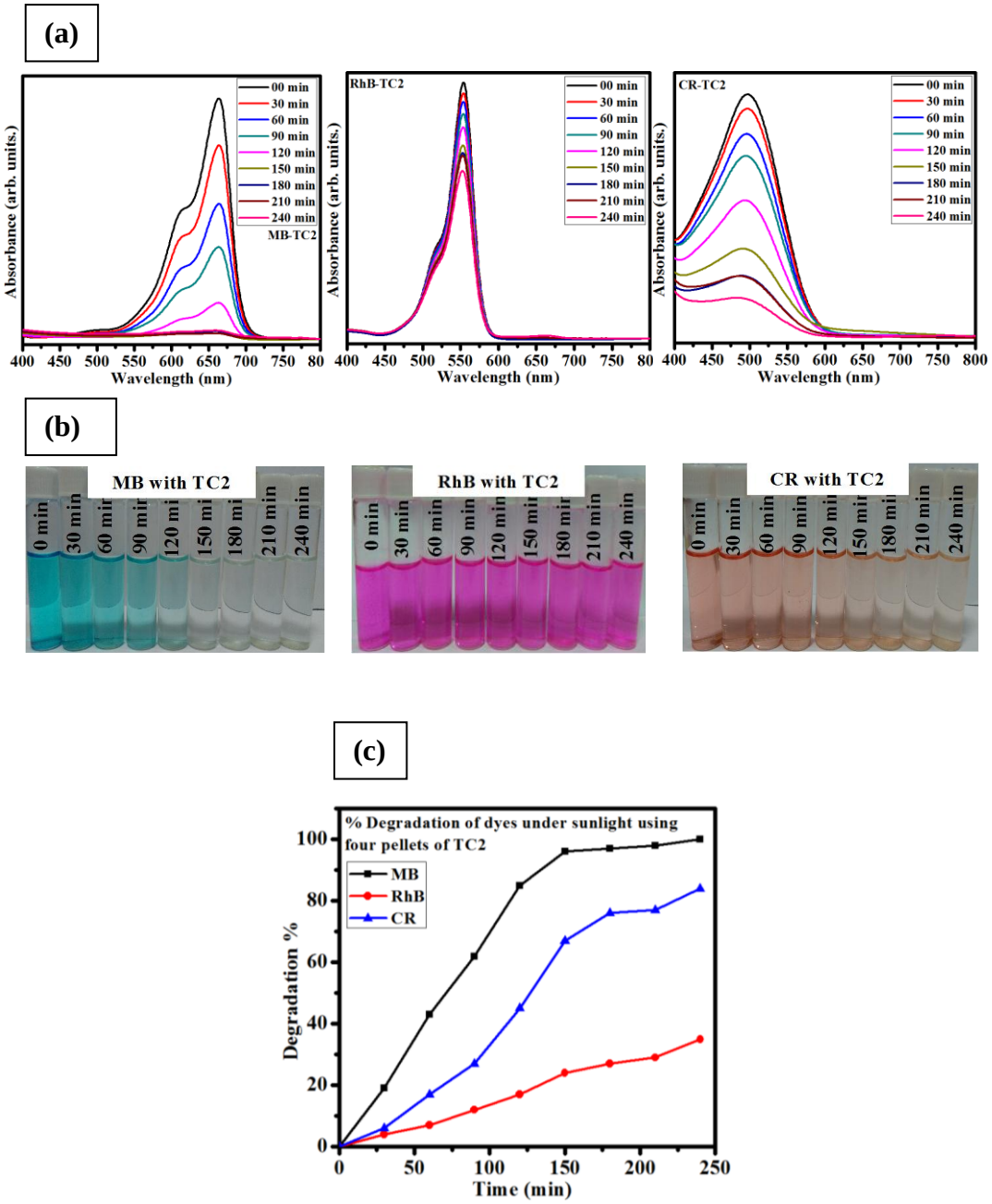

Figure 3.16 *(a) UV-visible absorption spectra of MB, (b) RhB and (c) CR, dye solutions with pellet TC2 before and after irradiating with sunlight. Inset show the pictorial representation of dye solutions from 0 min to 240 min (left to right), (d) Degradation percentage of dyes.*

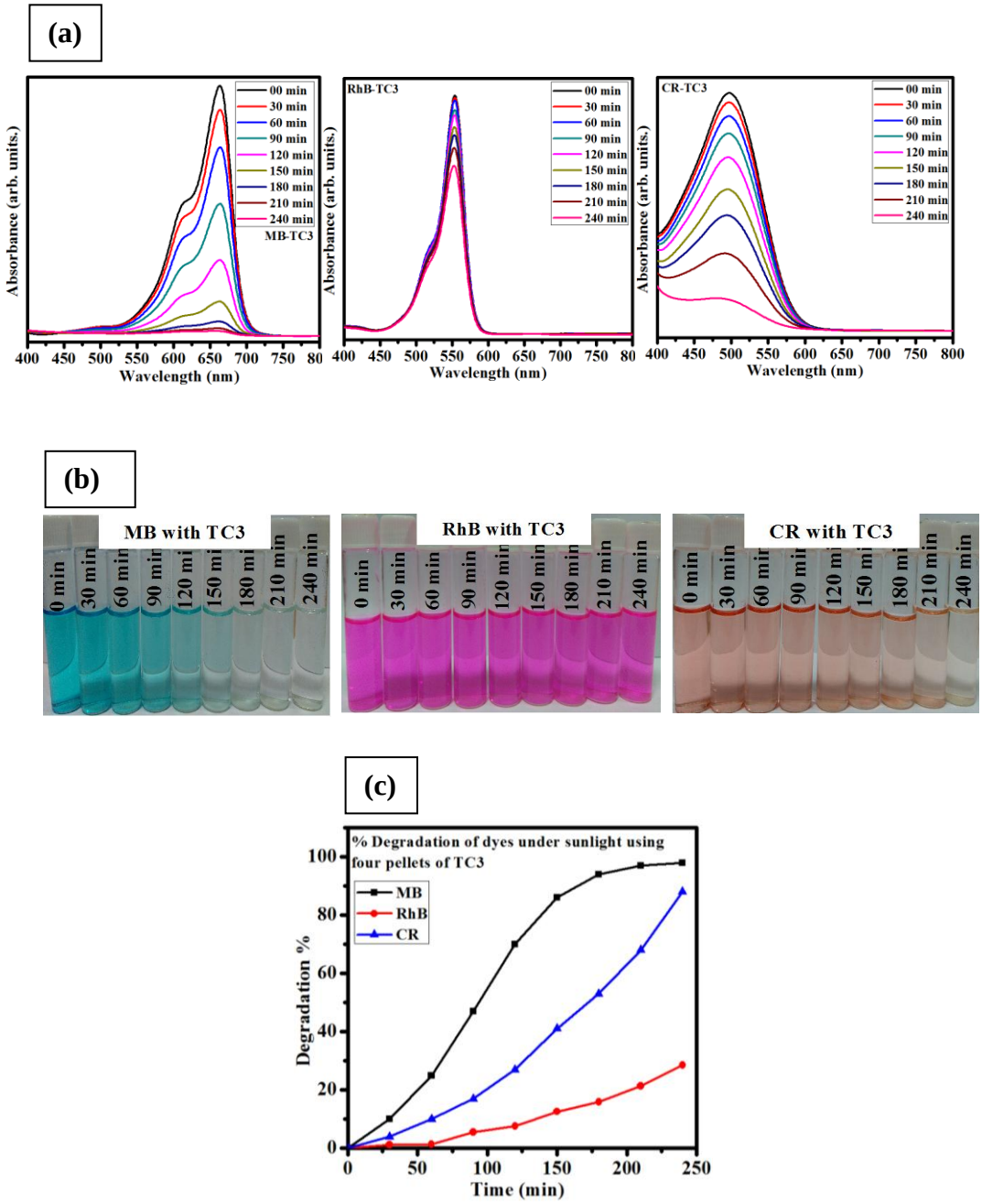

Figure 3.17 *(a) UV-visible absorption spectra of MB, RhB and CR, dye solutions with pellet TC3 before and after irradiating with sunlight. (b) show the pictorial representation of dye solutions from 0 min to 240 min (left to right), (c) Degradation percentage of dyes.*

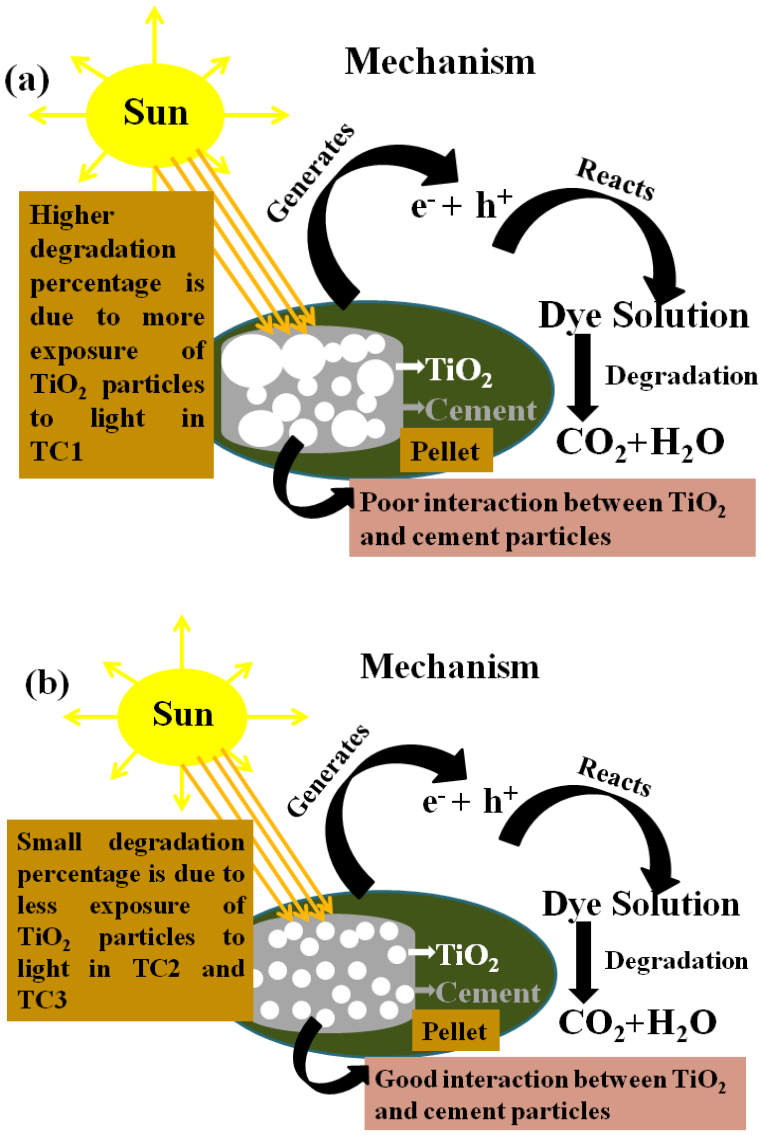

Figure 3.18 *Schematic diagram for mechanism of photocatalysis using cement and TiO_2 pellets, (a) TC1 and (b) TC2 and TC3 under sunlight.*

dioxide and water. The mechanism of photocatalytic degradation of dyes using the TC1 and TC2/TC3 pellets are shown in Figure 3.18.

It is well known that TiO_2 holds outstanding photocatalytic degradation ability. However, due to nanosize nature, it faces challenges in practical application such as cleaning of flowing waste water, separation of catalyst from purified water and repetitive use of

catalysts. Therefore, many research groups have put great effort in modifying the photocatalysis process for enhanced practical applications [Zhang et al. (2011)a, Bagwasi et al. (2013) and Niu et al. (2013)]. The study of TiO_2 photocatalyst with cement for self cleaning has surged remarkably for waste water purification [Cardenas et al. (2012), Rao et al. (2003), Janus et al. (2015) and Zhao et al. (2015)]. The degradation of NO_x gases during photocatalytic oxidation process using TiO_2 embedded cement-based materials have been assessed by Sugranez et al. (2013) and Cardenas et al. (2012). There are different reports available in literature regarding cement based composites of TiO_2 and their photocatalytic behavior. Janus et al. (2015) demonstrate the self-cleaning property of TiO_2-N,C loaded cementitious materials by degrading the dye Reactive Red 198. Immobilize TiO_2 with pumice stone prepared for photocatalytic transformations of organic pollutants in aqueous solution offering an economical process by reducing the cost of filtration [Rao et al. (2003)]. Such self cleaning processes make use of UV-light which is harmful for living organisms. Nevertheless, in our case, we avoid predominantly UV light by utilizing sunlight as renewable energy source. This process provides an inexpensive and facile methodology for water purification allowing repeated use of the material to a good extent which certainly minimizes the man power.

3.6 Conclusions

Anatase phase TiO_2 nanoparticles synthesized by sol-gel technique and studied the photocatalytic properties. The photocatalytic activity was undertaken by examining the degradation behavior of most common organic dyes such as MB, CR and RhB after illuminating with UV light as well as sunlight. We found that 100% degradation, of MB and

RhB after 180 min, whereas, CR degraded after 120 min under UV-irradiation. However, under sunlight it takes 90, 45 and 180 min for ~ 100% degradation of MB, CR and RhB**,** respectively. Further we fabricated TiO_2 and cement composite pellets with three different compositions and studied its photocatalytic property. The photocatalytic property was evaluated by degrading the dyes MB, RhB and CR in the presence of sunlight. A single pellet containing 50 mg of TiO_2 could degrade ~100% of CR and MB in 120 min of irradiation. On the other hand, four pellets containing 20 and 10 mg of TiO_2 showed ~85 to 100% degradation of CR and MB after 240 min of irradiation. RhB was degraded only ~30% irrespective of TiO_2 content in composite pellets. Though pellet with 50 mg TiO_2 revealed a high photocatalytic performance, it dissociated partially, whereas, pellets with 20 and 10 mg TiO_2 remain stable during the photocatalytic process. It is concluded that pellets with low TiO_2 contents than that of cement are more appropriate for practical application.